International Journal of Heat and Mass Transfer 147 (2020) 118917

Contents lists available at ScienceDirect

International Journal of Heat and Mass Transfer

journal homepage: www.elsevier.com/locate/ijhmt

Nonlinear thermal conductivity of periodic composites

Gaole Dai, Jiping Huang

Department of Physics, State Key Laboratory of Surface Physics, and Key Laboratory of Micro and Nano Photonic Structures (MOE), Fudan University, Shanghai 200433, China

ARTICLE INFO

Article history:
Received 13 May 2019
Received in revised form 14 September 2019
Accepted 17 October 2019

ABSTRACT

Composites have been widely used to realize various functions in thermal metamaterials, thus becoming important to predict heat transport properties according to geometric structures and component materials. Based on a first-principles approach, namely, the Rayleigh method, here we develop an analytical way to calculate temperature-dependent (i.e., nonlinear) thermal conductivities of a composite with circular inclusions arranged in a periodic rectangular array. We focus on both weak and strong nonlinearity. As a result, we find that the temperature-dependence (nonlinearity) coefficient of the whole periodic composite can be larger than that of the nonlinear component inside this composite. Simulation results from finite element analysis show that the Rayleigh method can be also more accurate than the Maxwell-Garnett or Bruggeman effective medium approximations. As a model application, we further tailor the nonlinearity to design a thermal diode, for which heat flux along one direction is much larger than that along the opposite. This work provides a different theory for handling periodic structure with thermally responsive thermal conductivities, and it could be useful for designing thermal metamaterials with diverse properties including rectification.

1. Introduction

The efficient utilization of thermal energy is important for human beings in the modern society. Since the transformation thermotics theory for heat conduction was proposed in 2008 [1,2], employing all kinds of composites with a specific thermal conductivity distribution has been a useful method for modulating the flow of heat, such as thermal cloaks, transparency or illusions [2–20], and concentrating, bending or rotating of heat flux [4,21–24]. Meanwhile, researchers have applied different kinds of effective medium approximations (EMAs) to calculate effective thermal conductivities of composites, including the well-known Maxwell-Garnett (M&G) formula [25] and Bruggeman formula [26], and their extended forms [27–33]. However, temperature-dependent (i.e., nonlinear) thermal conductivities have seldom been touched in macroscopic heat transfer although such nonlinear phenomena are common in the real world and nonlinearity in microscopic heat conduction has raised much interest [34–38]. From theoretical analysis to experimental measurements, many materials have been found to have temperature-dependent thermal conductivities [39–45]. Besides, based on various kinds of multi-layered or core-shell structures, nonlinearity (temperature-dependence) can induce potential applications in macroscopic heat management, such as switchable cloaks or concentrators [9,46], macroscopic thermal diodes [9], and energy-free or negative-energy-consumption maintenance of constant temperatures [47,48]. Nevertheless, other structures with nonlinearity, especially a periodic array embedded in a host, have not been investigated in the literature. In particular, such periodic arrays (with nonlinearity) might be important for real applications, as inspired by the fact that periodic structures (without nonlinearity) have been extensively investigated in the field of thermocrystals [49].

As an attempt, here we investigate two-dimensional periodic thermal composites with nonlinear thermal conductivities. We develop the method proposed by Lord Rayleigh [50] to calculate the effective nonlinear thermal conductivity of the periodic composites and search for the conditions where nonlinearity enhancement can happen. Here "nonlinearity enhancement" means that the nonlinearity coefficient of the whole periodic composite can be larger than that of the nonlinear component inside this composite. We start from weak nonlinearity and then investigate strongly nonlinear cases. We assume that the total thermal conductivity can be written as a sum of a constant and a temperature-dependent part. The weak nonlinearity means the constant part is much larger than the temperature-dependent part for all possible temperatures while the strongly nonlinear cases means the opposite situation. Finite-element simulations from commercial software COMSOL Multiphysics [51] show that the Rayleigh method can be more accurate than M&G or Bruggeman EMAs for circular inclusions especially when the concentration of inclusions is high enough. Finally we design a thermal diode using strong nonlinearity with both homogeneous material and periodic composites.

E-mail address: jphuang@fudan.edu.cn (J. Huang)

https://doi.org/10.1016/j.ijheatmasstransfer.2019.118917
0017-9310/

2. Theory

Consider two-dimensional periodic composites where the inclusions are circular and form a rectangular array, and denote κ_j and p_j as the thermal conductivity and area fraction of the jth component. Here, $j = i$ or h is respectively for the inclusion or host. Obviously we have $f_i + f_h = 1$ where f_i and f_h denote the area fraction of the inclusion and the host respectively. If we assume that either the inclusion or host is nonlinear materials with a thermal conductivity dependent on temperature (T), κ_j can be written as

$$\kappa_j = \kappa_{j0} + \chi_j (T + T_{\mathrm{rt}})^{\alpha} \quad (j = i, h). \tag{1}$$

Here κ_{j0} is the linear (namely, temperature-independent) part of κ_j, χ_j is the nonlinearity (temperature-dependence) coefficient, T_{rt} is the reference temperature for measuring nonlinearity and α should be a real number. From the Debye approximation at low temperatures, the thermal conductivity of solids is proportional to T^3 ($\alpha = 3$) while at high temperatures the Eucken's law tells $\alpha \approx -1$ for many cases [42,43]. Callaway [44] developed a lattice model and predicted $\alpha = -3/2$ for normal germanium and $\alpha = -2$ for single-isotope germanium from 50 K to 100 K, which are in good accordance with the experimental results. Sometimes $\alpha = 1$ can be a good approximation for measurement data of copper and ingot iron [45].

For simplicity, we consider two cases as shown in Fig. 1: $\chi_h = 0$ and $\chi_i \neq 0$ in Fig. 1(a); $\chi_h \neq 0$ and $\chi_i = 0$ in Fig. 1(b). In principle, thermal conductivities should vary as the temperature changes due to different microscopic mechanisms. If the nonlinearity is weak [namely, $\chi_j (T + T_{\mathrm{rt}})^{\alpha} \ll \kappa_{j0}$ in Eq. (1)], the effective conductivity of the composite material can be simply written as

$$\kappa_e = \kappa_{e0} + \chi_e (T + T_{\mathrm{rt}})^{\alpha} + O[(T + T_{\mathrm{rt}})^{2\alpha}], \tag{2}$$

where κ_{e0} is the linear solution, χ_e is the effective nonlinearity coefficient, and $O[(T + T_{\mathrm{rt}})^{2\alpha}]$ denote higher-order terms which are all smaller than $\chi_e (T + T_{\mathrm{rt}})^{\alpha}$. In other words, if we take the term $O[(T + T_{\mathrm{rt}})^{\alpha}]$ as first-order infinitesimal compared with $\kappa_0, O[(T + T_{\mathrm{rt}})^{2\alpha}]$ is the second-order infinitesimal. To see the enhancement or reduction of nonlinearity, we define the nonlinearity coefficient ratio as

$$c = \frac{\chi_e}{\chi_j} \tag{3}$$

where $j = i$ for the first case (i.e., only the inclusions are nonlinear: $\chi_i \neq 0$ and $\chi_h = 0$) while $j = h$ for the second (namely, only the host is nonlinear: $\chi_h \neq 0$ and $\chi_i = 0$). It's obvious that the enhancement of nonlinearity means $c > 1$. In addition, the coefficient c can help us match the required thermal conductivity when using composites to design thermal metamaterials. For example, thermal cloaks, concentrators and rotators have been realized in experiments for linear conduction using composites. When nonlinear effects exist, the matching of nonlinearity coefficient should also be considered. In the following part, we will develop the Rayleigh method to calculate c and also use EMAs for the sake of comparison.

2.1. The Rayleigh method

The Rayleigh method [50] is a first-principles approach to the effective conductivity of periodic composites especially for spherical and cylindrical inclusions. It uses the Rayleigh identity to obtain an approximate solution of the Laplace equation and has been successfully applied in electricity or electromagnetism to calculate both linear and nonlinear conductivities [52–58]. Here we follow the framework of Ref. [58] which studied nonlinear electrical media, in order for us to extend the Rayleigh method to periodic nonlinear thermal composites. Here some remarks should be added. In nonlinear electricity, usually the nonlinear electrical conductivity is directly dependent on the electrical field or the power of its absolute value while the nonlinear thermal conductivity directly relies on temperature, rather than its gradient (which is just mathematically analogous to electric fields in nonlinear electricity). This fact brings new physics and great difference when extending from nonlinear electricity to nonlinear thermotics (as discussed in this work).

To proceed, we assume that two heat sources (see Fig. 1) with separation L and temperatures T_L and T_R are respectively put on the left and right boundary of the composites. First we consider the linear case and denote the temperature distribution as T_0. The zeroth-order equation for temperature is (note $j = i$ and h for the inclusion and host, respectively)

$$\nabla \cdot (\kappa \nabla T_0^j) = 0, \tag{4}$$

which is a homogeneous Laplace equation for T_0^j.

In polar coordinates (ρ, θ), the general solution for Laplace equation is [59]

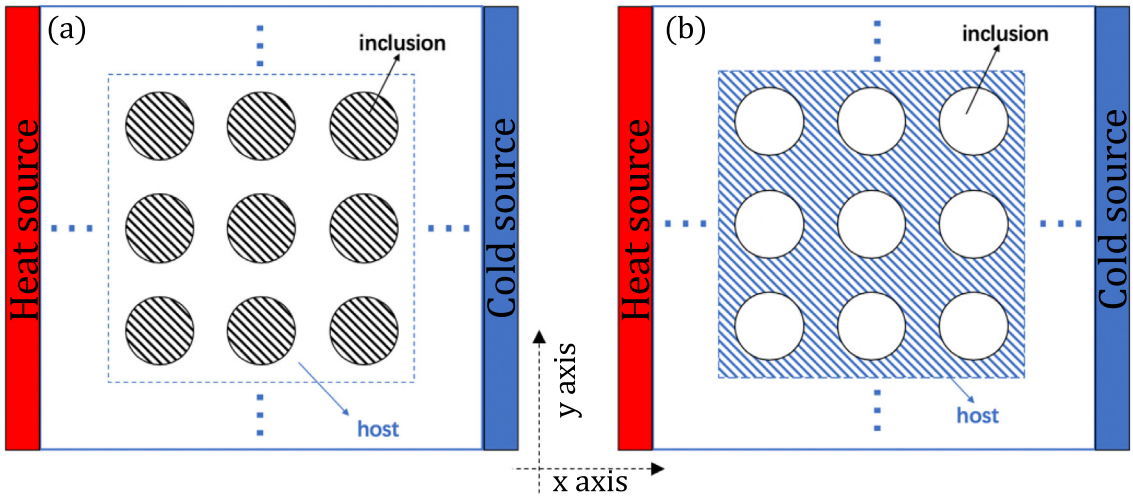

Fig. 1. Schematic diagram illustrating two classes of periodic composites: circles denote the inclusions and shadow lines represent the material with a nonlinear (temperature-dependent) thermal conductivity. (a) nonlinear inclusions are periodically embedded in a linear (temperature-independent) host; (b) linear inclusions are periodically embedded in a nonlinear host. Also, we put a hot source (the red panel) on the left side and a cold source (blue panel) on the right.

$$(A_0 + B_0 \ln\rho)(\mu_0 + v_0\theta) + \sum_{m=1}^{\infty}(A_m\rho^m + B_m\rho^{-m})\left[\mu_m \sin(m\theta) + v_m\cos(m\theta)\right] \tag{5}$$

and we set the pole O or the point $(0,0)$ at the center of a selected cell in the composite. Since we set the temperature gradient along the x direction, so $B_0 = v_0 = 0$. In addition, the temperature should always has a finite value when ρ is finite, so we should exclude the terms ρ^{-m} for the general solution in the inclusions since the point $\rho = 0$ is in the inclusion, meaning

$$T_0^i(\rho,\theta) = C_{00} + \sum_{m=1}^{\infty} C_{0m}^2\rho^m\cos(m\theta) + C_{0m}^1\rho^m\sin(m\theta). \tag{6}$$

In the host, we can also write

$$T_0^h(\rho,\theta) = A_{00} + \sum_{m=1}^{\infty}(A_{0m}^2\rho^m + B_{0m}^2\rho^{-m})\cos(m\theta) + (A_{0m}^1\rho^m + B_{0m}^1\rho^{-m})\sin(m\theta). \tag{7}$$

To solve out the coefficient sets $A_{00}, A_{0m}^2, A_{0m}^1, B_{0m}^1, B_{0m}^2, C_{00}, C_{0m}^1$ and C_{0m}^2, we resort to both the boundary conditions between the inclusions and host (boundaries denoted as $\partial\Gamma$)

$$T_0^i = T_0^h|_{\partial\Gamma}, \tag{8a}$$

$$\kappa_i\frac{\partial T_0^i}{\partial\rho} = \kappa_h\left.\frac{\partial T_0^h}{\partial\rho}\right|_{\partial\Gamma}, \tag{8b}$$

and the Rayleigh identity [53,54,58]

$$A_{00} + \sum_{m=1}^{\infty}\rho^m[A_{0m}^2\cos(m\theta) + A_{0m}^1\sin(m\theta)] = \sum_{k=1}^{\infty}\sum_{m=1}^{\infty}\rho_k^{-m}[B_{0m}^2\cos(m\theta_k) + B_{0m}^1\sin(m\theta_k)] - \tfrac{T_L-T_R}{L}x. \tag{9}$$

Here θ_k is the angular coordinate in another polar coordinate system whose pole O_k is the center of the k-th cell and we can also denote ρ_k as the corresponding radial coordinate. If we take x_k and y_k as the Cartesian coordinates of the center in the k-th cell, we can write

$$\rho_k = \sqrt{(x-x_k)^2 + (y-x_k)^2}, \tag{10a}$$

$$\cos\theta_k = (x-x_k)/\rho_k. \tag{10b}$$

Note that the integer index k is positive while the polar coordinate we use at the beginning in Eq. (5) has its pole in the 0-th cell.

Now we turn to Eq. (7). The terms with ρ^m increase with larger ρ so they represent the influence on temperature originating from infinity and inclusions except the one in the 0-th cell. On the other hand, the terms with ρ^{-m} should be connected with the inclusion in the 0-th cell because they increase with decreasing ρ and is singular at $\rho = 0$. We can do a further subdivision and write T_0^h as [53,54,58]

$$T_0^h = \sum_{m=1}^{\infty}\rho^{-m}[B_{0m}^2\cos(m\theta) + B_{0m}^1\sin(m\theta)] + \sum_{k=1}^{\infty}\sum_{m=1}^{\infty}\rho_k^{-m}[B_{0m}^2\cos(m\theta_k) + B_{0m}^1\sin(m\theta_k)] - \tfrac{T_L-T_R}{L}x. \tag{11}$$

Again, the term $\sum_{m=1}^{\infty}\rho^{-m}[B_{0m}^2\cos(m\theta) + B_{0m}^1\sin(m\theta)]$ comes from the inclusion in the 0-th cell and $\sum_{m=1}^{\infty}\rho_i^{-m}[B_{0m}^2\cos(m\theta_k) + B_{0m}^1\sin(m\theta_k)]$ comes from the k-th ($k>0$) and satisfies spatial periodic-translation invariance. In addition, $-\frac{T_L-T_R}{L}x$ corresponds to heat sources at infinity and it would be the exact solution when there are no inclusions. Because Eq. (7) and Eq. (11) must give the same result, we can easily get the Rayleigh identity Eq. (9). Also we can find the Rayleigh identity is a conclusion of superposition theorem for linear differential equation since the three parts of Eq. (11) all satisfy the Laplace equation Eq. (4).

As contrast, when only one particle is embedded or the inclusions are very dilute, the boundary condition at infinity is often used instead of the Rayleigh identity. By partially differentiating with respect to x in both sides and taking the value at point Q (which can be arbitrary with Cartesian or polar coordinates being (x,y) or (ρ,θ)), the Rayleigh identity gives [58]

$$\sum_{m=1}^{\infty}\tfrac{m!\rho^{m-n}(\kappa_h+\kappa_i)}{(m-n)!(\kappa_h-\kappa_i)}[A_{0m}^2\cos((m-n)\theta) + A_{0m}^1\sin((m-n)\theta)] - \sum_{m=1}^{\infty}(-1)^n\tfrac{(m+n-1)!}{(m-1)!}\times[B_{0m}^2W_{m+n}^2(Q) + B_{0m}^1W_{m+n}^1(Q)] = -\tfrac{T_L-T_R}{L}\delta_{1,n} \tag{12}$$

where

$$\delta_{1,n} = \begin{cases} 1 & (n=1) \\ 0 & (n\neq 1)\end{cases}, \tag{13a}$$

$$W_l^1(Q) = \sum_{k=1}^{\infty}\rho_k^{-l}\sin(l\theta_k), \tag{13b}$$

$$W_l^2(Q) = \sum_{k=1}^{\infty}\rho_k^{-l}\cos(l\theta_k). \tag{13c}$$

By truncating the series expansions [we only need to keep $A_{01}^2, A_{03}^2, B_{01}^2$ and B_{03}^2 in Eq. (12) for the lowest approximation because only the odd values of m can exist when the temperature gradient is applied along the x direction while the even terms isn't consistent with the parity], we can write the approximate solutions in the selected cell as

$$T_0^i(\rho,\theta) = C_{00} + C_{01}^2\rho\cos\theta + C_{03}^2\rho^3\cos(3\theta) \tag{14}$$

and

$$T_0^h(\rho,\theta) = C_{00} + A_{01}^2\rho\cos\theta + A_{03}^2\rho^3\cos(3\theta) + B_{01}^2\rho^{-1}\cos\theta + B_{03}^2\rho^{-3}\cos(3\theta), \tag{15}$$

where [58]

$$B_{01}^2 = -\frac{T_L-T_R}{L}/(\frac{\kappa_h+\kappa_i}{a^2(\kappa_h-\kappa_i)} - \frac{3a^6(W_4^2)^2(\kappa_h-\kappa_i)}{\kappa_h+\kappa_i}), \tag{16a}$$

$$B_{03}^2 = -\frac{a^6W_4^2(\kappa_h-\kappa_i)}{\kappa_h+\kappa_i})B_{01}^2, \tag{16b}$$

$$A_{0m}^2 = \frac{\kappa_h+\kappa_i}{a^{2m}(\kappa_h-\kappa_i)}B_{0m}^2, \tag{16c}$$

$$C_{0m}^2 = \frac{2\kappa_h}{a^{2m}(\kappa_h-\kappa_i)}B_{0m}^2, \tag{16d}$$

$$W_4^2 = 3.13085/S^2. \tag{16e}$$

Here a is the radius of a single particle in the unit cell with area S. The only difference from the electrical counterpart is that C_{00} is usually neglected in electricity because a constant term in electrical potentials should not change the corresponding physical properties. Fortunately, in the linear case, C_{00} (though still to be determined by more conditions) should not influence the result of effective conduction, too. Also, $W_4^2(Q)$ doesn't depend on the choice of Q and it's related to the shape of lattices [53,54]. The coefficients C_{0m}^2 in Eq. (16d) are actually calculated by the boundary condition Eq. (8) in the 0-th cell so if we take the values of C_{0m}^2 into Eq. (14), we get the solution of for the inclusion in the 0-th cell (with C_{00} not determined). For inclusions in k-th cell, because the system is periodic, we can reselect the k-th cell as the new 0-th one.

The effective thermal conductivity κ_e can be calculated by [60,61]

$$\kappa_e = \kappa_h + (\kappa_i - \kappa_h)\langle \nabla_x T_0 \rangle_i / \langle \nabla_x T_0 \rangle, \tag{17}$$

where $\langle \dots \rangle$ means the spatial average and $\langle \dots \rangle_i$ means the integral over inclusions divided by the whole volume of the composite. It is easy to see

$$\langle \nabla_x T_0 \rangle_i = C_{01}^2 f_i, \tag{18}$$

$$f_i = \pi a^2 / S. \tag{19}$$

Note there exists a relationship from self-consistent field method [58]

$$\langle \nabla_x T_0 \rangle = -\frac{2\kappa_h}{\kappa_h + \kappa_e} \frac{T_L - T_R}{L}. \tag{20}$$

Then we can find that the effective thermal conductivity has the same form as its electrical counterpart in the case of linear conduction, namely,

$$\kappa_e = \kappa_h \times \frac{(-\beta_1 + \beta_1 f_i + f_i^4)\kappa_h^2 - 2(\beta_1 + f_i^4)\kappa_h \kappa_i + (-\beta_1 - \beta_1 f_i + f_i^4)\kappa_i^2}{(-\beta_1 - \beta_1 f_i + f_i^4)\kappa_h^2 - 2(\beta_1 + f_i^4)\kappa_h \kappa_i + (-\beta_1 + \beta_1 f_i + f_i^4)\kappa_i^2}, \tag{21}$$

where $\beta_1 = 3.31248$ (which equals to $\frac{\pi^4}{3(W_4^2 S^2)^2}$).

However, for the nonlinear case, it could be much more complicated if we still follow the way of calculating electrical conductivity in Ref. [58], using Rayleigh identity (for nonlinear conduction) combined with perturbation theory to solve a nonhomogeneous equation. The difficulty results from the fact that the thermal conductivity depends on the temperature (i.e., potential) while the electrical conductivity relies on the field (namely, the gradient of potential). Nevertheless, we can take Eq. (1) into Eq. (21) and use Taylor series to calculate c through

$$c = \frac{\partial \kappa_e}{\chi_j (T + T_{\mathrm{rt}})^{\alpha} \partial \chi_j}. \tag{22}$$

Finally, the expressions of c for the two cases we study are

$$c = \frac{4\beta_1 f_i \kappa_{h0}^2 \left[\beta_1 (\kappa_{h0} + \kappa_{i0})^2 + f_i^4 (\kappa_{h0} - \kappa_{i0})^2\right]}{\left[\beta_1 (\kappa_{h0} + \kappa_{i0})(f_i \kappa_{h0} - f_i \kappa_{i0} + \kappa_{h0} + \kappa_{i0}) - f_i^4 (\kappa_{h0} - \kappa_{i0})^2\right]^2} \tag{23}$$

for the first case and

$$c = \frac{-\beta_1^2 (f_i - 1)(\kappa_{h0} + \kappa_{i0})^2 \left[(f_i + 1)\kappa_{h0}^2 - 2(f_i - 1)\kappa_{h0}\kappa_{i0} + (f_i + 1)\kappa_{i0}^2\right]}{\left[\beta_1 (\kappa_{h0} + \kappa_{i0})(f_i \kappa_{h0} - f_i \kappa_{i0} + \kappa_{h0} + \kappa_{i0}) - f_i^4 (\kappa_{h0} - \kappa_{i0})^2\right]^2} + \frac{-2\beta_1 f_i^4 (\kappa_{h0} - \kappa_{i0})^2 \left[2(f_i + 1)\kappa_{h0}\kappa_{i0} + \kappa_{h0}^2 + \kappa_{i0}^2\right] + f_i^8 (\kappa_{h0} - \kappa_{i0})^4}{\left[\beta_1 (\kappa_{h0} + \kappa_{i0})(f_i \kappa_{h0} - f_i \kappa_{i0} + \kappa_{h0} + \kappa_{i0}) - f_i^4 (\kappa_{h0} - \kappa_{i0})^2\right]^2} \tag{24}$$

for the second case. It can be easily confirmed that c only depends on area fraction f_i and ratio κ_{i0}/κ_{h0}. In addition, the expressions of c keep the same for different α and T_{rt}, two additional parameters as adopted in Eq. (1).

2.2. Effective medium approximation (EMA)

The EMA is another method to calculate the effective properties of composites. Although EMA is usually seen as an approximation which applies to various disordered systems, recent works show that it can work well in some periodic systems [18,62]. Here we resort to the M&G formula and Bruggeman formula respectively [30]

$$\frac{\kappa_e - \kappa_h}{\kappa_e + \kappa_h} = f_i \frac{\kappa_i - \kappa_h}{\kappa_i + \kappa_h}, \tag{25a}$$

$$f_i \frac{\kappa_e - \kappa_i}{\kappa_e + \kappa_i} + f_h \frac{\kappa_e - \kappa_h}{\kappa_e + \kappa_h} = 0. \tag{25b}$$

Again, take the expression of nonlinear conductivity, named Eq. (1), into Eq. (25a) and Eq. (25b) respectively. Then, by cutting off the series expansions of Eq. (2), we obtain

$$\chi_e (T + T_{\mathrm{rt}})^{\alpha} = \frac{\partial \kappa_e}{\partial \chi_i} \tag{26}$$

where κ_e is a function of κ_{j0}, f_j and χ_j. For the first case, only the inclusion is nonlinear and then the nonlinearity coefficient ratio c $(= \chi_e/\chi_i)$ is given by

$$c = \frac{4 f_i}{\left(1 + \frac{\kappa_{i0}}{\kappa_{h0}} + f_i - f_i \frac{\kappa_{i0}}{\kappa_{h0}}\right)^2} \tag{27}$$

from the M&G formula and

$$c = \frac{1}{2}\left[\frac{(2f_i - 1)\left(2f_i - 2f_i \frac{\kappa_{h0}}{\kappa_{i0}} - 1 + \frac{\kappa_{h0}}{\kappa_{i0}}\right) + 2\frac{\kappa_{h0}}{\kappa_{i0}}}{\sqrt{\left(2f_i - 2f_i \frac{\kappa_{h0}}{\kappa_{i0}} - 1 + \frac{\kappa_{h0}}{\kappa_{i0}}\right)^2 + 4\frac{\kappa_{h0}}{\kappa_{i0}}}} + 2f_i - 1\right] \tag{28}$$

from the Bruggeman formula. For the second case where only the host is nonlinear, we can also obtain the nonlinearity coefficient ratio c $(= \chi_e/\chi_h)$ as

$$c = \frac{(1 - f_i^2)\left[1 + \left(\frac{\kappa_{i0}}{\kappa_{h0}}\right)^2\right] + 2(1 - f_i)^2 \frac{\kappa_{i0}}{\kappa_{h0}}}{\left(1 + \frac{\kappa_{i0}}{\kappa_{h0}} + f_i - f_i \frac{\kappa_{i0}}{\kappa_{h0}}\right)^2} \tag{29}$$

from the M&G formula and

$$c = \frac{1}{2}\left[\frac{(2f_i - 1)\left(2f_i - 2f_i \frac{\kappa_{i0}}{\kappa_{h0}} - 1 + \frac{\kappa_{i0}}{\kappa_{h0}}\right) + 2\frac{\kappa_{i0}}{\kappa_{h0}}}{\sqrt{\left(2f_i - 2f_i \frac{\kappa_{i0}}{\kappa_{h0}} - 1 + \frac{\kappa_{i0}}{\kappa_{h0}}\right)^2 + 4\frac{\kappa_{i0}}{\kappa_{h0}}}} - 2f_i + 1\right] \tag{30}$$

from the Bruggeman formula. Again, the values of α and T_{rt} do not change the form of c according to our derivation.

2.3. Strong nonlinearity

So far, we have set the nonlinearity to be weak, namely, $\chi_j (T + T_{\mathrm{rt}})^{\alpha} \ll \kappa_{j0}$ in Eq. (1). Generally speaking, it is difficult to establish an analytical theory to calculate the effective conductivity for all cases especially when linear and nonlinear parts are comparable. Strong nonlinearity is another case that we might apply the Rayleigh method. Below we give a brief discussion.

Thermal conductivities sometimes can vary dramatically for the change of temperature, such as metals with phase changes (say, gallium) and shape-memory alloy. For the latter, its effective thermal conductivity changing with temperature can be approximately described by a logistic function, which has been used to design thermal metamaterials in [9,47,48]. For electrical composites with strong nonlinearity (neglecting the linear term), Gao and Li developed a self-consistent mean-field method to calculate effective electrical conductivities [63,64]. However, since the nonlinear thermal conductivity relies on temperature (potential) rather than its gradient (field), we need to develop a different method. Let us use the methods above to deal with this problem. Consider the case that both the host and inclusions have thermal conductivities with strong nonlinearity $\chi_j (T + T_{\mathrm{rt}})^{\alpha} \gg \kappa_{j0}$, Eq. (1) can be written as

$$\kappa_j = \kappa_{j0} + \chi_j (T + T_{\mathrm{rt}})^{\alpha} \approx \chi_j (T + T_{\mathrm{rt}})^{\alpha} \quad (j = i, h). \tag{31}$$

In this case, the effective thermal conductivity calculated by the Rayleigh method, M&G formula and Bruggeman formula has the same form as

$$\kappa_e = \chi_e (T + T_{\mathrm{rt}})^{\alpha}. \tag{32}$$

Taking Eq. (31) into Eq. (21) and Eq. (25) respectively, we can see from the Rayleigh method that

$$\chi_e = \chi_h \frac{(-\beta_1+\beta_1 f_i+f_i^4)\chi_h^2 - 2(\beta_1+f_i^4)\chi_h\chi_i + (-\beta_1-\beta_1 f_i+f_i^4)\chi_i^2}{(-\beta_1-\beta_1 f_i+f_i^4)\chi_h^2 - 2(\beta_1+f_i^4)\chi_h\chi_i + (-\beta_1+\beta_1 f_i+f_i^4)\chi_i^2}, \tag{33}$$

Meanwhile, the M&G formula yields

$$\chi_e = \chi_h \frac{\chi_h(1-f_i) + \chi_i(1+f_i)}{\chi_h(1+f_i) + \chi_i(1-f_i)}, \tag{34}$$

and the Bruggeman formula gives

$$\chi_e = \frac{1}{2}\left[\sqrt{(1-2f_i)^2(\chi_h-\chi_i)^2 + 4\chi_h\chi_i} + (1-2f_i)(\chi_h-\chi_i)\right]. \tag{35}$$

Clearly, we can observe that Eqs. (33)–(35) have the same forms as the corresponding linear cases if we replace χ_h and χ_i by κ_h and κ_i, respectively.

3. Comparing analytical theories with finite-element simulations

To evaluate our analytic solutions derived from the Rayleigh method and EMA, we compare them with the simulation results

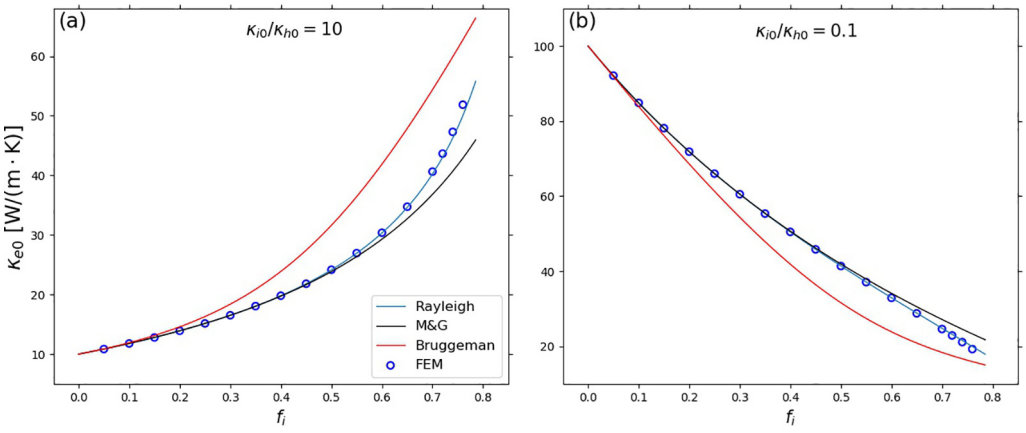

Fig. 2. The linear part of effective thermal conductivity κ_{e0} (or effective linear condcutivity) versus concentration f_i. In (a), we take $\kappa_{i0} = 100$ W/(m·K) and $\kappa_{h0} = 10$ W/(m·K) while $\kappa_{i0} = 10$ W/(m·K) and $\kappa_{h0} = 100$ W/(m·K) in (b). The light blue, black and red lines respectively represent the analytical predictions of the Rayleigh method, M&G formula and Bruggeman formula. The scatter plot of blue circles shows the finite-element simulation results.

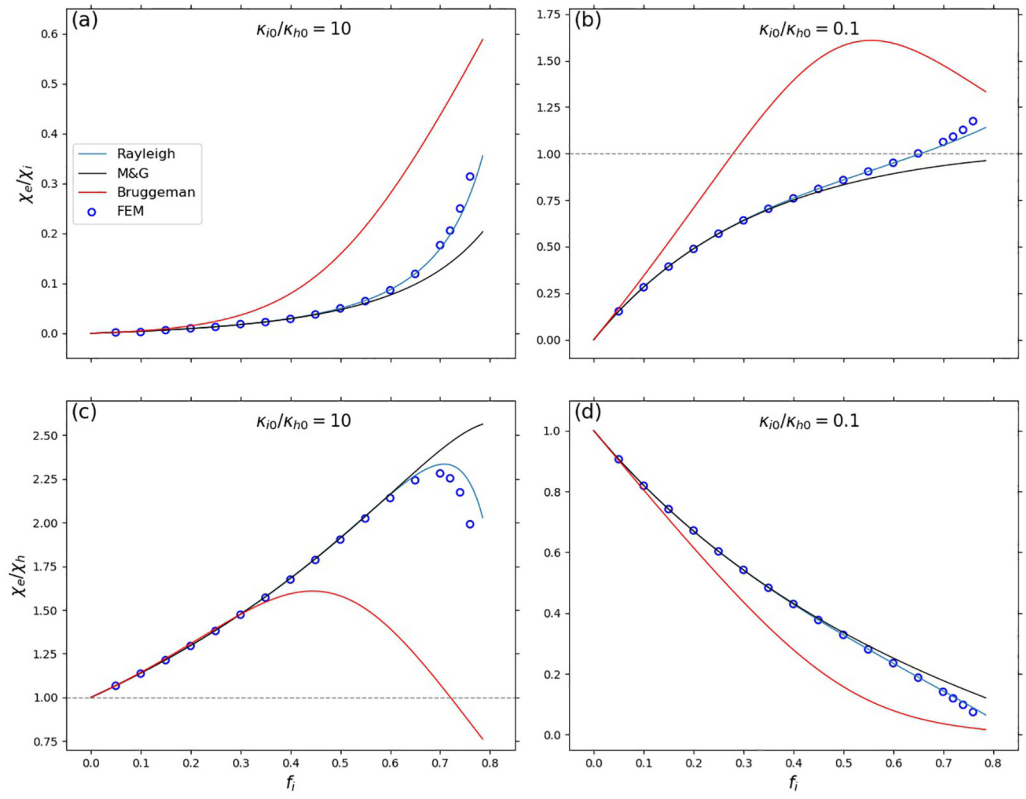

Fig. 3. Nonlinearity coefficient ratio as a function of f_i. (a) and (b) corresponds to Fig. 1(a) where only the inclusions are nonlinear while (c) and (d) corresponds to Fig. 1(b) where only the host is nonlinear. In (a), $\kappa_h = 10$ W/(m · K) and $\kappa_i = 100$ W/(m · K) $+\left[0.01\mathrm{W}/(\mathrm{m}\cdot\mathrm{K}^2)\right] \times T$. In (b), $\kappa_h = 100$ W/(m · K) and $\kappa_i = 10$ W/(m · K) $+\left[0.001\mathrm{W}/(\mathrm{m}\cdot\mathrm{K}^2)\right] \times T$. In (c), $\kappa_h = 10$ W/(m · K) $+\left[0.001\mathrm{W}/(\mathrm{m}\cdot\mathrm{K}^2)\right] \times T$ and $\kappa_i = 100$ W/(m · K). In (d), $\kappa_h = 100$ W/(m · K) $+\left[0.01\mathrm{W}/(\mathrm{m}\cdot\mathrm{K}^2)\right] \times T$ and $\kappa_i = 10$ W/(m · K).

obtained from the commercial finite-element method software COMSOL Multiphysics. In our model, the size of the whole composite material is 20 cm × 20 cm and that of each unit cell is 1 cm × 1 cm. In addition, the two heat sources put on boundaries are set as $T_L = 313$ K and $T_R = 273$ K. Since the shape of inclusions is circle, there is an upper limit of area fraction $f_i < \pi/4$ if no overlapping exists. Also, without loss of generality, we take $\alpha = 1$ and $T_{rt} = 0$ K if not stated otherwise.

When considering weak nonlinearity, Fig. 2 and Fig. 3 respectively show the effective linear thermal conductivity κ_{e0} and nonlinearity coefficient ratio c for two different κ_{i0}/κ_{h0} ratios. First, we look at the results in Fig. 2, which shows the effective linear thermal conductivity κ_{e0} as a function of f_i. For Fig. 2(a), we take $\kappa_{i0}/\kappa_{h0} = 10$ while $\kappa_{i0}/\kappa_{h0} = 0.1$ for Fig. 2(b). We can see κ_{e0} is always between the values of κ_{i0} and κ_{h0}, and the Rayleigh method appears to be more accurate than the two EMAs (M&G formula and Bruggeman formula), especially for large values of f_i. This is because the two EMAs are derived from the assumption that the inclusions are randomly distributed and the multipolar interactions (beyond dipolar interactions) between inclusions are neglected. However, the Rayleigh method consider such interactions within periodic structures by taking the Rayleigh identity as part of the boundary conditions.

In Fig. 3, (a,b) show the nonlinearity coefficient ratio c for nonlinear inclusions embedded in a linear host [the first case illustrated by Fig. 1(a)] while (c,d) show the results for linear inclusions embedded in a nonlinear host [the second case illustrated by Fig. 1(b)]. The linear part of effective conductivity for Fig. 3(a,c) (taking $\kappa_{i0}/\kappa_{h0} = 10$) can be found in Fig. 3(a,c) and that for Fig. 3(b,d) (taking $\kappa_{i0}/\kappa_{h0} = 0.1$) can be found in Fig. 2(b). Again, we can find that the Rayleigh method provides better predictions than the two EMAs (especially for large values of f_i). What's more, different from composites with random-embedded inclusions [66], nonlinearity enhancement (corresponding to $c > 1$) can not only happen for $\chi_i = 0, \chi_h > 0$ and $\kappa_{i0}/\kappa_{h0} > 1$ [see Fig. 3(c)], but also for $\chi_i > 0, \chi_h = 0$ and $\kappa_{i0}/\kappa_{h0} < 1$ [see Fig. 3(b)], as long as f_i is large enough.

Also, for strong nonlinearity, we plot Fig. 4. We set $\chi_i/\chi_h = 5$ in Fig. 4 and $\chi_i/\chi_h = 1/5$ in Fig. 4(b). We can see that, like the weakly linear case, the Rayleigh method gives the most accurate predic-

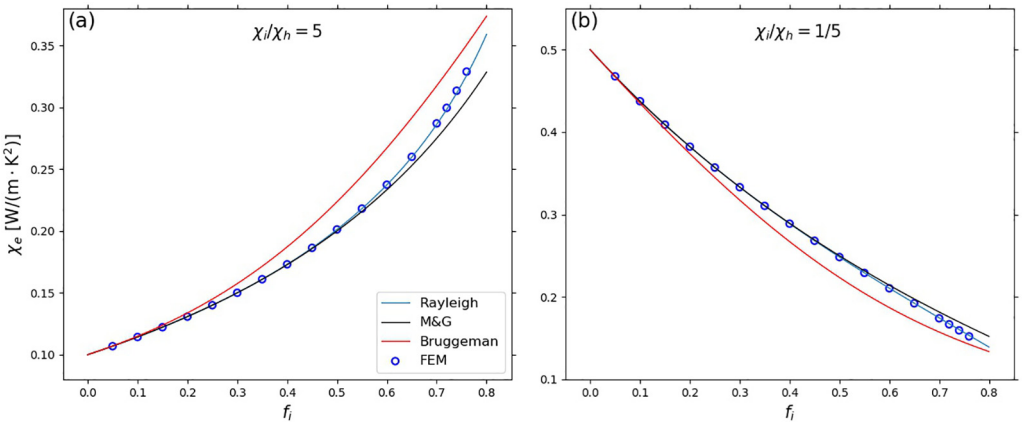

Fig. 4. Effective nonlinearity coefficient χ_e versus f_i for strong nonlinearity. Parameters: (a) $\chi_i = 0.5$ W/(m · K^2) and $\chi_h = 0.1$ W/(m · K^2); (b) $\chi_i = 0.1$ W/(m · K^2) and $\chi_h = 0.5$ W/(m · K^2).

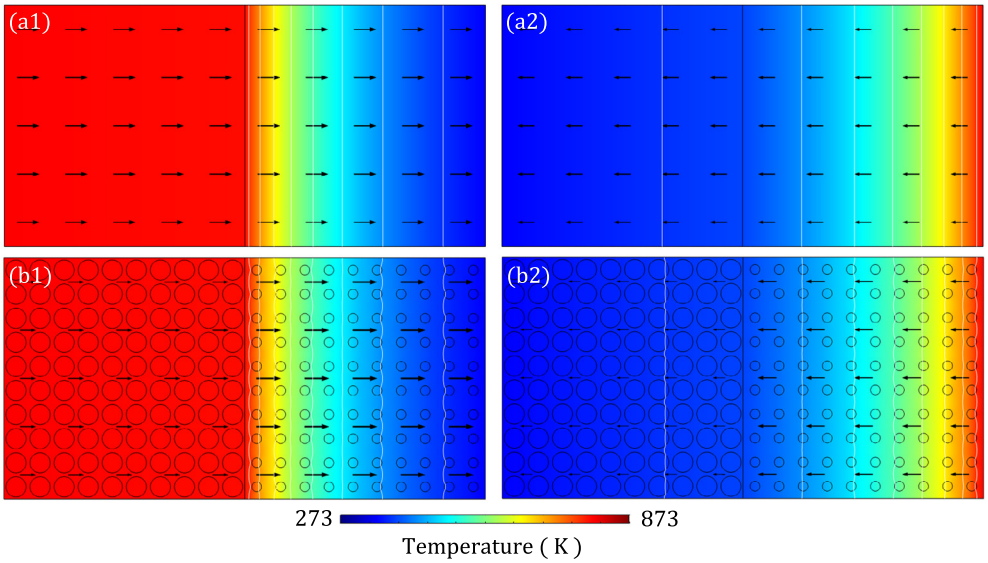

Fig. 5. Design schematics of two thermal diode expected to have the same rectification ratio. In (a), we use two homogeneous materials A and B. In (b), we use two periodic structures. Two kinds of inclusions, denoted by red and purple circles, are embedded into two host materials respectively. In both of (a) and (b), we put heat source with temperature T_L on the left (the green panel) and another with T_R on the right (the yellow panel). In (a), we set $\kappa_A = (T/100)^2$ [W/(m · K^3)] and $\kappa_B = (500/T)^2$ [W · K/m]. In (b), we set $\kappa_{A,host} = 0.5(T/100)^2$ [W/(m · K^3)], $\kappa_{A,inclusion} = 2(T/100)^2$ [W/(m · K^3)] and $f_{iA} = 55.00\%$ in the left part. For the right part, we set $\kappa_{B,host} = 1.2(500/T)^2$ [W · K/m], $\kappa_{B,inclusion} = 0.2(500/T)^2$ [W · K/m] and $f_{iB} = 12.73\%$.

tions. In addition, χ_e increases as f_i increases in Fig. 4(a) while the behavior is opposite in Fig. 4(b), just as what effective linear conductivities do in Fig. 2.

It is known that strong nonlinearity and asymmetry can be a useful tool to achieve rectification effect [34,9,65] from micro to macro scales. Here, considering Fourier's law for macroscopic heat conduction, we design a toy thermal diode using materials satisfying Eq. (31). We follow the work in Ref [65], utilizing two materials (namely, A and B) whose conductivities have different power-law-exponent relationships α with temperature. The schematic design is shown in Fig. 5(a), which is a two-segment bar with material A on the left part and B on the right. Each material occupies a 0.1 m $\times$ 0.1 m square area. Again, temperatures T_L, T_R are set on the left and right boundaries respectively. To generate the rectification effect, we set $\kappa_A = (T/100)^2$ [W/(m $\cdot$ K^3)] and $\kappa_B = (500/T)^2$ [W $\cdot$ K/m]. Also, to check the Rayleigh method in a more specific case, we use periodic structure to match κ_A, κ_B. As illustrated in Fig. 5(b), we use four materials in another diode which has the same size and boundary conditions as the one in Fig. 5(a). In its left part, corresponding to material A, we set the conductivity of the host as $\kappa_{A,host} = 0.5(T/100)^2$ [W/(m $\cdot$ K^3)]. The conductivity of the inclusion is $\kappa_{A,inclusion} = 2(T/100)^2$ [W/(m $\cdot$ K^3)] and the area fraction of the inclusions $f_{i,A}$ calculated by the Rayleigh method is 55.00%. Also, for the right part, we set $\kappa_{B,host} = 1.2(500/T)^2$ [W $\cdot$ K/m], $\kappa_{\mathrm{B,inclusion}} = 0.2(500/\mathrm{T})^2$ [W $\cdot$ K/m] and area fraction $f_{i,B}$ is 12.73%. We hope the two diodes in Fig. 5 can have the same rectification ratio ψ defined by $\psi = |J^+ - J^-| / (J^+ + J^-)$. Here J^+ (or J^-) denotes the heat flux when heat flows from left to right (or from right to left) in the diode.

Setting cold/hot source with a temperature at 273 K/873 K, Fig. 6 illustrates the temperature distribution and heat flux of the two diodes. Fig. 6(a1-a2) is for the diode using homogeneous materials corresponding to Fig. 6 and Fig. 6(b1-b2) is for its counterparts using periodic composites corresponding to Fig. 5(b). In Fig. 6(a1) and (b1), $T_L = 873$ K and $T_R = 273$ K, while in Fig. 6(a2) and (b2), $T_L = 273$ K and $T_R = 873$ K. The white lines are isotherms and we can see the temperature distributions in Fig. 6(a1) and (b1) are very close. So are the temperature distributions in Fig. 6(a2) and (b2). The black arrows in Fig. 6 show the directions of heat flux and their lengths are proportional to the magnitudes of heat flux. Also, we can see the heat flow (arrow) in (a1)/(b1) is larger than that in (a2)/(b2), thus yielding the behavior of rectification. The rectification ratio for (a1) and (a2) is 13.26% and 13.28% for (b1) and (b2). We can find they are almost the same since the periodic

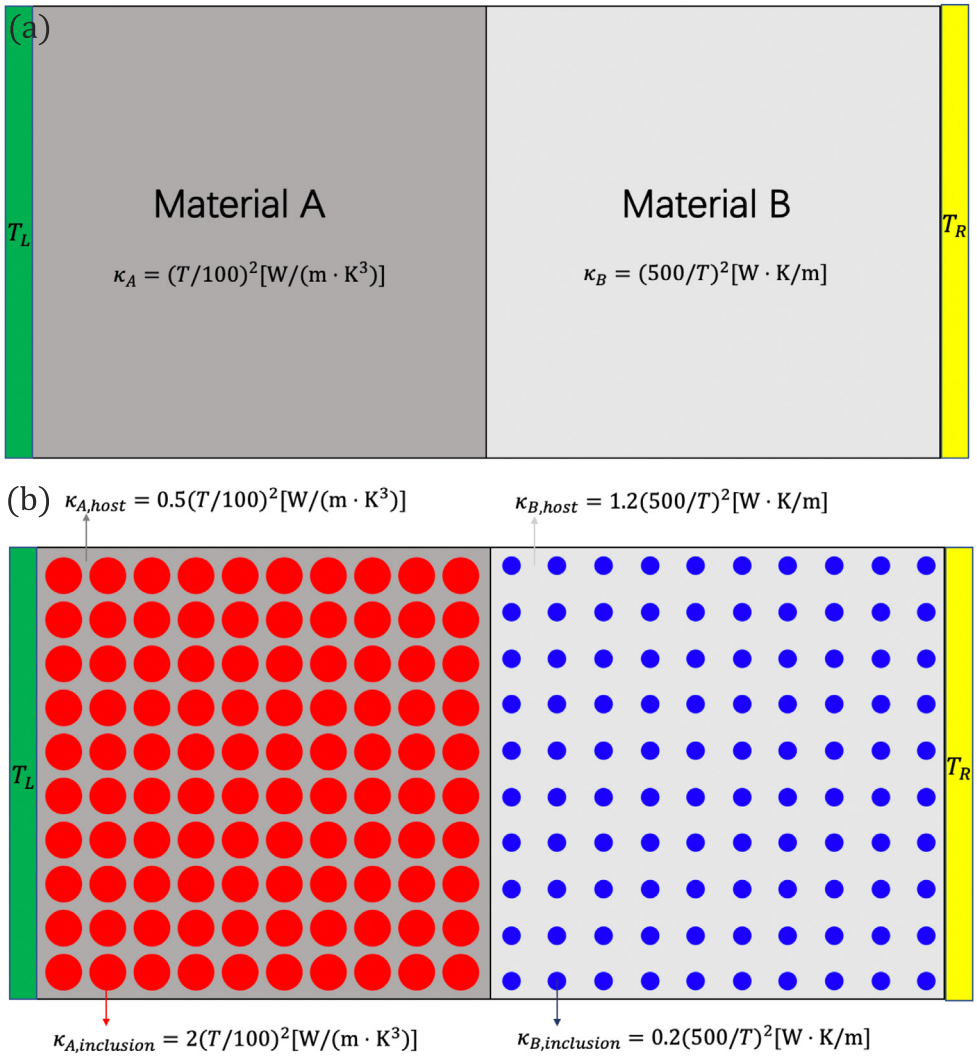

Fig. 6. (a1-a2) show temperature distributions and heat flux for the design corresponding to Fig. 5 and (b1-b2) show those for Fig. 5(b). In (a1) and (b1) [or (a2) and (b2)], the left end is set at 873 K [or 273 K] and the right 273 K [or 873 K]. The white lines are isotherms. The black arrows represent the direction of heat flux, and the length of the arrows denotes the magnitude of heat flux.

composites should have equivalent effective conductivities as material A and B. The heat flows, for example, in (a1) and (b1) look not the same because (b1) only draws the flow in the host due to some settings in COMSOL Multiphysics. However, when considering the total flux in both inclusions and host, (b1) (or (a1)) has about the same heat flow as (b2) (or (a2)), which is in consistence with the conclusion on rectification ratio.

4. Discussion and conclusion

Without loss of generality, we have adopted the square lattice in our thermal composite. In fact, the Rayleigh method can still work for other lattices, such as the hexagonal lattice. The only difference is that the coefficient in Eq. (16e) should be numerically recalculated by using Eq. (13c) according to the specific lattice in use [67].

We can see from Figs. 2–4 that M&G formula can also work well when f_i is not large. Here we want to give a brief discuss on the relationship of M&G formula and the Rayleigh method. The M&G formula comes from a condition that [30]

$$\langle \nabla_x T_0^i \rangle = \frac{2\kappa_h}{\kappa_h + \kappa_i} \langle \nabla_x T_0^h \rangle. \tag{36}$$

Here, for simplicity, we don't distinguish κ_j from κ_{j0} $(j = i, h)$. Since the outer temperature gradient is put along the x direction, the approximation $\langle \nabla_x T_0^h \rangle \approx -\frac{T_L - T_R}{L}$ is reasonable in M&G theory. If we consider inclusions with conductivity κ_e, we can find Eq. (36) turns similar to Eq. (20). Also, we can find in M&G theory,

$$\langle \nabla_x T_0^i \rangle = -\frac{2\kappa_h}{\kappa_h + \kappa_i} \frac{T_L - T_R}{L}, \tag{37}$$

while in Rayleigh method, Eq. (18) tells

$$\langle \nabla_x T_0^i \rangle = -\frac{2\kappa_h(\kappa_h + \kappa_h)}{(\kappa_h + \kappa_i)^2 - 0.301888 f_i^4 (\kappa_h - \kappa_i)^2} \frac{T_L - T_R}{L}. \tag{38}$$

Then we can find the two expressions above for $\langle \nabla_x T_0^i \rangle$ should become the same if $0.301888 f_i^4 (\kappa_h - \kappa_i)^2 / (\kappa_h + \kappa_i)^2$ can be neglected. Area fraction f_i plays the main role here as it has a fourth-power relationship and can be much smaller than 1 when itself is not big. This can explain why M$G formula can also give nice predictions in Figs. 2–4 within a certain range. Nevertheless, from the point of view of the entire range of f_i, predictions from the Rayleigh method can be more accurate and have a wider and more general applicability for periodic composites, as confirmed by the finite-element simulations.

In summary, we have employed the Rayleigh method to investigate the nonlinear thermal conductivity in composites with periodic structures and revealed the conditions for nonlinearity enhancement. Also, we have investigated both weak and strong nonlinearity. In this work, we have considered two-dimensional composites with circular inclusions and this method can be extended to three-dimensional cases whose inclusions may be cylindrical, spherical or even elliptical-cylindrical, based on the results of their linear counterparts by the Rayleigh method [55–57]. This method is helpful to make intricate and precise designs of thermal metamaterials by tailoring nonlinear conductivities, such as thermal diodes, and it is also useful for other areas including nonlinear electromagnetic periodic composites.

Declaration of Competing Interest

The authors declare that there are no conflicts of interest.

Acknowledgment

We appreciate useful discussions with Mr. J. Wang and Mr. C. R. Jiang, and acknowledge the financial support by the National Natural Science Foundation of China under Grant No. 11725521.

References

[1] C.Z. Fan, Y. Gao, J.P. Huang, Shaped graded materials with an apparent negative thermal conductivity, Appl. Phys. Lett. 92 (2008), 251907.
[2] T. Chen, C.N. Weng, J.S. Chen, Cloak for curvilinearly anisotropic media in conduction, Appl. Phys. Lett. 93 (2008), 114103.
[3] J.Y. Li, Y. Gao, J.P. Huang, A bifunctional cloak using transformation media, J. Appl. Phys. 108 (2010), 074504.
[4] S. Narayana, Y. Sato, Heat flux manipulation with engineered thermal materials, Phys. Rev. Lett. 108 (2012), 214303.
[5] R. Schittny, M. Kadic, S. Guenneau, M. Wegener, Experiments on transformation thermodynamics: molding the flow of heat, Phys. Rev. Lett. 110 (2013), 195901.
[6] X. He, L.Z. Wu, Thermal transparency with the concept of neutral inclusion, Phys. Rev. E 88 (2013), 033201.
[7] T. Han, X. Bai, J.T.L. Thong, B. Li, C.W. Qiu, Full control and manipulation of heat signatures: cloaking, camouflage and thermal metamaterials, Adv. Mater. 26 (2014) 1731.
[8] X.Y. Shen, J.P. Huang, Thermally hiding an object inside a cloak with feeling, Int. J. Heat Mass Transfer 78 (2014) 1.
[9] Y. Li, X.Y. Shen, Z.H. Wu, J.Y. Huang, Y.X. Chen, Y.S. Ni, J.P. Huang, Temperature-dependent transformation thermotics: From switchable thermal cloaks to macroscopic thermal diodes, Phys. Rev. Lett. 115 (2015), 195503.
[10] Y.X. Liu, W.L. Guo, T.C. Han, Arbitrarily polygonal transient thermal cloaks with natural bulk materials in bilayer configurations, Int. J. Heat Mass Transfer 115 (2017) 1.
[11] S.L. Zhou, R. Hu, X.B. Luo, Thermal illusion with twinborn-like heat signatures, Int. J. Heat Mass Transfer 127 (2018) 607.
[12] J. Guo, Z.G. Qu, Thermal cloak with adaptive heat source to proactively manipulate temperature field in heat conduction process, Int. J. Heat Mass Transfer 127 (2018) 1212.
[13] R.Z. Wang, J. Shang, J.P. Huang, Design and realization of thermal camouflage with many-particle systems, Int. J. Therm. Sci. 131 (2018) 14.
[14] J. Shang, C.R. Jiang, L.J. Xu, J.P. Huang, Many-particle thermal invisibility and diode from effective media, J. Heat Transfer 140 (2018), 092004.
[15] Y. Li, X. Bai, T.Z. Yang, H.L. Luo, C.W. Qiu, Structured thermal surface for radiative camouflage, Nat. Commun. 9 (2018) 273.
[16] R. Hu, S.L. Zhou, Y. Li, D.Y. Lei, B.X. Luo, C.W. Qiu, Illusion thermotics, Adv. Mater. 30 (2018) 1707237.
[17] Y. Li, K.J. Zhu, Y.G. Peng, W. Li, T.Z. Yang, H.X. Xu, H. Chen, X.F. Zhu, S.H. Fan, C. W. Qiu, Thermal meta-device in analogue of zero-index photonics, Nat. Mater. 18 (2019) 48.
[18] L.J. Xu, C.R. Jiang, J. Shang, R.Z. Wang, J.P. Huang, Periodic composites: quasi-uniform heat conduction, Janus thermal illusion, and illusion thermal diodes, Eur. Phys. J. B 90 (2017) 221.
[19] L.J. Xu, S. Yang, J.P. Huang, Thermal theory for heterogeneously architected structure: Fundamentals and application, Phys. Rev. E 98 (2018), 052128.
[20] L.J. Xu, S. Yang, J.P. Huang, Designing effective thermal conductivity of materials of core-shell structure: theory and simulation, Phys. Rev. E 99 (2019), 022107.
[21] R.S. Kapadia, P.R. Bandaru, Heat flux concentration through polymeric thermal lenses, Appl. Phys. Lett. 105 (2014), 233903.
[22] T.Z. Yang, K.P. Vemuri, P.R. Bandaru, Experimental evidence for the bending of heat flux in a thermal metamaterial, Appl. Phys. Lett. 105 (2014), 083908.
[23] K.P. Vemuri, P.R. Bandaru, Anomalous refraction of heat flux in thermal metamaterials, Appl. Phys. Lett. 104 (2014), 083901.
[24] K.P. Vemuri, F.M. Canbazoglu, P.R. Bandaru, Guiding conductive heat flux through thermal metamaterials, Appl. Phys. Lett. 105 (2014), 193904.
[25] J.C.M. Garnett, Colours in metal glasses and in metallic films, Philos. Trans. R. Soc. London Ser. A 203 (1904) 385.
[26] D.A.G. Bruggeman, Calculation of various physics constants in heterogenous substances: Dielectricity constants and conductivity of mixed bodies from isotropic substances, Ann. Phys., Leipzig 24 (1935) 636.
[27] T.K. Xia, P.M. Hui, D. Stroud, Theory of Faraday rotation in granular magnetic materials, J. Appl. Phys. 67 (1990) 2736.
[28] C.Y. You, S.C. Shin, S.Y. Kim, Modified effective-medium theory for magneto-optical spectra of magnetic materials, Phys. Rev. B 55 (1997) 5953.
[29] O. Levy, D. Stroud, Maxwell-Garnett theory for mixtures of anisotropic inclusions: application to conducting polymers, Phys. Rev. B 56 (1997) 8035.
[30] J.P. Huang, K.W. Yu, Enhanced nonlinear optical responses of materials: composite effects, Phys. Rep. 431 (2006) 87.
[31] L.H. Shi, L. Gao, Subwavelength imaging from a multilayered structure containing interleaved nonspherical metal-dielectric composites, Phys. Rev. B 77 (2008), 195121.
[32] D.H. Liu, C. Xu, P.M. Hui, Effects of a coating of spherically anisotropic material in core-shell particles, Appl. Phys. Lett. 92 (2008), 181901.
[33] K.P. Vemuri, P.R. Bandaru, Geometrical considerations in the control and manipulation of conductive heat flux in multilayered thermal metamaterials, Appl. Phys. Lett. 113 (2013), 133111.

[34] B.W. Li, L. Wang, G. Casati, Thermal diode: Rectification of heat flux, Phys. Rev. Lett. 93 (2004), 184301.
[35] B.W. Li, L. Wang, G. Casati, Negative differential thermal resistance and thermal transistor, Appl. Phys. Lett. 88 (2006), 143501.
[36] L. Wang, B.W. Li, Thermal logic gates: computation with phonons, Phys. Rev. Lett. 99 (2007), 177208.
[37] P. Ben-Abdallah, S.A. Biehs, Near-field thermal transistor, Phys. Rev. Lett. 112 (2014), 044301.
[38] V. Kubytskyi, S.A. Biehs, P. Ben-Abdallah, Radiative bistability and thermal memory, Phys. Rev. Lett. 113 (2014), 074301.
[39] C.J. Glassbrenner, G.A. Slack, Thermal conductivity of silicon and germanium from 3K to the melting point, Phys. Rev. 134 (1964) A1058.
[40] P.D. Maycock, Thermal conductivity of silicon, germanium, III–V compounds and III–V alloys, Solid State Electron. 10 (1967) 161.
[41] R.C. Zeller, R.O. Pohl, Thermal conductivity and specific heat of noncrystalline solids, Phys. Rev. B 4 (1971) 2029.
[42] L.D. Landau, E.M. Lifshitz, Statistical Physics Part 1, 3rd ed., Pergamon Press, New York, 1980.
[43] G.Z. Qin, Z.Z. Qin, H.M. Wang, M. Hu, Anomalously temperature-dependent thermal conductivity of monolayer GaN with large deviations from the traditional 1/T law, Phys. Rev. B 95 (2017), 195416.
[44] J. Callaway, Model for lattice thermal conductivity at low temperatures, Phys. Rev. 113 (1958) 1046.
[45] L.J. Briggs, Gallium: Thermal conductivity; supercooling; negative pressure, J. Chem. Phys. 26 (1957) 784.
[46] Y. Li, X.Y. Shen, J.P. Huang, Y.S. Ni, Temperature-dependent transformation thermotics for unsteady states: Switchable concentrator for transient heat flow, Phys. Lett. A 380 (2016) 1641.
[47] X.Y. Shen, Y. Li, C.R. Jiang, J.P. Huang, Temperature trapping: Energy-free maintenance of constant temperatures as ambient temperature gradients change, Phys. Rev. Lett. 117 (2016), 055501.
[48] J. Wang, J. Shang, J.P. Huang, Negative energy consumption of thermostats at ambient temperature: Electricity generation with zero energy maintenance, Phys. Rev. Appl. 11 (2019), 024053.
[49] M. Maldovan, Narrow low-frequency spectrum and heat management by thermocrystals, Phys. Rev. Lett. 110 (2013), 025902.
[50] Lord Rayleigh, On the influence of obstacles arranged in rectangular order upon the properties of a medium, Philos. Mag. 34 (1892) 481.
[51] http://www.comsol.com/.
[52] R.E. Meredith, C.W. Tobias, Resistance to potential flow through a cubical array of spheres, J. Appl. Phys. 31 (1960) 1270.
[53] R.C. McPhedran, D.R. McKenzie, The conductivity of lattices of spheres I. The simple cubic lattice, Proc. R. Soc. London, Ser. A 359 (1978) 45.
[54] R.C. McPhedran, D.R. McKenzie, The conductivity of lattices of spheres II. The body centred and face centred cubic lattices, Proc. R. Soc. London, Ser. A 362 (1978) 211.
[55] N.A. Nicorovici, R.C. McPhedran, Transport properties of arrays of elliptical cylinders, Phys. Rev. E 54 (1996) 1945.
[56] J.G. Yardley, A.J. Reuben, R.C. McPhedran, The transport properties of layers of elliptical cylinders, Proc. R. Soc. London, Ser. A 457 (2001) 395.
[57] T.Y. Chen, H.Y. Kuo, Transport properties of composites consisting of periodic arrays of exponentially graded cylinders with cylindrically orthotropic materials, J. Appl. Phys. 98 (2005), 033716.
[58] G.Q. Gu, K.W. Yu, P.M. Hui, First-principles approach to conductivity of a nonlinear composite, Phys. Rev. B 58 (1998) 3057.
[59] A. Zangwill, Modern Electrodynamics, Cambridge University Press, UK, 2012.
[60] G.Q. Gu, K.W. Yu, Effective conductivity of nonlinear composites, Phys. Rev. B 46 (1992) 4502.
[61] K.W. Yu, G.Q. Gu, Effective conductivity of nonlinear composites. II. Effective-medium approximation, Phys. Rev. B 47 (1993) 7568.
[62] L.J. Xu, S. Yang, J.P. Huang, Thermal transparency induced by periodic interparticle interaction, Phys. Rev. Appl. 11 (2019), 034056.
[63] L. Gao, Z.Y. Li, Self-consistent formalism for a strongly nonlinear composite: comparison with variational approach, Phys. Lett. A 219 (1996) 324.
[64] L. Gao, Z.Y. Li, Effective response of a strongly nonlinear composite: comparison with variational approach, Phys. Lett. A 222 (1996) 207.
[65] C. Dames, Solid-state thermal rectification with existing bulk materials, J. Heat Transfer 131 (2009), 061301.
[66] G.L. Dai, J. Shang, R.Z. Wang, J.P. Huang, Nonlinear thermotics: nonlinearity enhancement and harmonic generation in thermal metasurfaces, Eur. Phys. J. B 9 (2018) 59.
[67] W.M. Suen, S.P. Wong, K. Young, The lattice model of heat conduction in a composite material, J. Phys. D 12 (1979) 1325.